

Wave attenuation across a tidal marsh in San Francisco Bay

M.R. Foster-Martinez^{a,*}, J.R. Lacy^b, M.C. Ferner^c, E.A. Variano^a

^a Civil and Environmental Engineering, University of California, Berkeley, United States

^b U.S. Geological Survey Pacific Coastal and Marine Science Center, United States

^c San Francisco Bay National Estuarine Research Reserve, San Francisco State University, United States

ARTICLE INFO

Keywords:

Salt marsh

Wave attenuation

Coastal protection

Spartina foliosa

Salicornia pacifica

San Francisco Bay

ABSTRACT

Wave attenuation is a central process in the mechanics of a healthy salt marsh. Understanding how wave attenuation varies with vegetation and hydrodynamic conditions informs models of other marsh processes that are a function of wave energy (e.g. sediment transport) and allows for the incorporation of marshes into coastal protection plans. Here, we examine the evolution of wave height across a tidal salt marsh in San Francisco Bay. Instruments were deployed along a cross-shore transect, starting on the mudflat and crossing through zones dominated by *Spartina foliosa* and *Salicornia pacifica*. This dataset is the first to quantify wave attenuation for these vegetation species, which are abundant in the intertidal zone of California estuaries. Measurements were collected in the summer and winter to assess seasonal variation in wave attenuation. Calculated drag coefficients of *S. foliosa* and *S. pacifica* were similar, indicating equal amounts of vegetation would lead to similar energy dissipation; however, *S. pacifica* has much greater biomass close to the bed (<20 cm) and retains biomass throughout the year, and therefore, it causes more total attenuation. *S. foliosa* dies back in the winter, and waves often grow across this section of the marsh. For both vegetation types, attenuation was greatest for low water depths, when the vegetation was emergent. For both seasons, attenuation rates across *S. pacifica* were the highest and were greater than published attenuation rates across similar (*Spartina alterniflora*) salt marshes for the comparable depths. These results can inform designs for marsh restorations and management plans in San Francisco Bay and other estuaries containing these species.

1. Introduction

Marshes, and tidal salt marshes in particular, are gaining recognition as critical elements in sustainable shoreline protection (Spalding et al., 2014a, 2014b; Narayan et al., 2016a; Narayan et al., 2016b; Green Infrastructure Effectiveness Database, 2017; Vuik et al., 2016). They contribute to coastal resiliency not only by attenuating wave energy in large storms (Gedan et al., 2011; Möller et al., 2014), but also by maintaining the existence of coastal land (Kirwan et al., 2016), supporting fisheries (Boesch and Turner, 1984; MacKenzie and Dionne, 2008), sequestering carbon (Ouyang and Lee, 2014), and removing contaminants (Dhir et al., 2009; Windham et al., 2003). These benefits directly contribute to the sustainability of the growing populations in coastal regions (Sutton-Grier et al., 2015). With this recognition, there are many ongoing projects to preserve existing salt marshes, restore former marshes, and create hybrids of natural and engineered structures (Pontee et al., 2016). These projects require an understanding of the underpinning processes that lead to marsh sustainability. One key process is wave

attenuation.

Marsh plants attenuate wave energy via frictional drag. This drag has an impact on the overall wave evolution to a greater or lesser degree depending on vegetation and hydrodynamic characteristics (e.g. storm track and speed (Wamsley et al., 2010) and vegetation patchiness (Temmerman et al., 2012)). Understanding how attenuation changes with these conditions informs our understanding of other marsh processes that are influenced by wave energy, such as sediment transport and deposition. Lower wave energy can create conditions conducive to sediment trapping and settling, which is critical to marsh survival. Wave attenuation across marshes has been studied in both the field and laboratory. Tables containing aggregated results can be found in Paquier et al. (2016), Guannel et al. (2015), and Gedan et al. (2011).

It is well established that marshes attenuate wave energy, but the degree of attenuation can greatly vary. Pinsky et al. (2013) reprocessed data from nine field studies on marshes using a uniform method. The calculated drag coefficient (C_D), which is a measure of attenuation, ranged from 0.5 to 30 for similar hydrodynamic conditions. This

* Corresponding author. Louisiana State University, Center for Coastal Resiliency, United States.

E-mail address: madeline@berkeley.edu (M.R. Foster-Martinez).

variability is in part due to the presence of different vegetation species and location-specific conditions (e.g. tidal range, offshore bathymetry, bed characteristics). Cooper (2005) lists 23 factors that influence wave attenuation, many of which varied across the marshes in Pinsky's analysis. The ways that these factors combine in a location drive the spatial and temporal patterns of marsh effects on waves. Therefore, local measurements focusing on sites of interest are necessary for effective resource management and shoreline protection.

In this study, we measured wave attenuation in a tidal salt marsh in San Francisco Bay. The most abundant salt marsh species present are *Salicornia pacifica* (pickleweed) and *Spartina foliosa* (Pacific cordgrass) (Baye, 2012). *S. pacifica* and *S. foliosa* are morphologically different; *S. foliosa* is rod-like, while *S. pacifica* is shorter and highly branched (i.e. more shrub-like). The existing wave attenuation literature has focused heavily on *Spartina alterniflora* (smooth cordgrass), as it is dominant along the east coast of the U.S. and the Gulf of Mexico (e.g. (Knutson

et al., 1982) in the field and (Anderson and Smith, 2014) in a flume). *S. foliosa* is distinct from *S. alterniflora* mainly because it is shorter and has less leaf production (Callaway and Josselyn, 1992). We also examined the seasonal variation in wave attenuation. Both *S. pacifica* and *S. foliosa* are perennial species; however, the aboveground biomass of *S. foliosa* dies back in the winter months, while *S. pacifica* retains aboveground biomass year-round.

The goal of this paper is to provide a first look at the wave attenuation and its seasonal variation across vegetated marshes in San Francisco Bay. We investigated how wave attenuation varies as waves progress through the different vegetation zones, as well as how it varies within the zones under different hydrodynamic conditions. We calculated bulk drag coefficients and exponential decay constants to differentiate mechanisms of dissipation. Finally, we discuss the results in the context of projected sea-level rise.

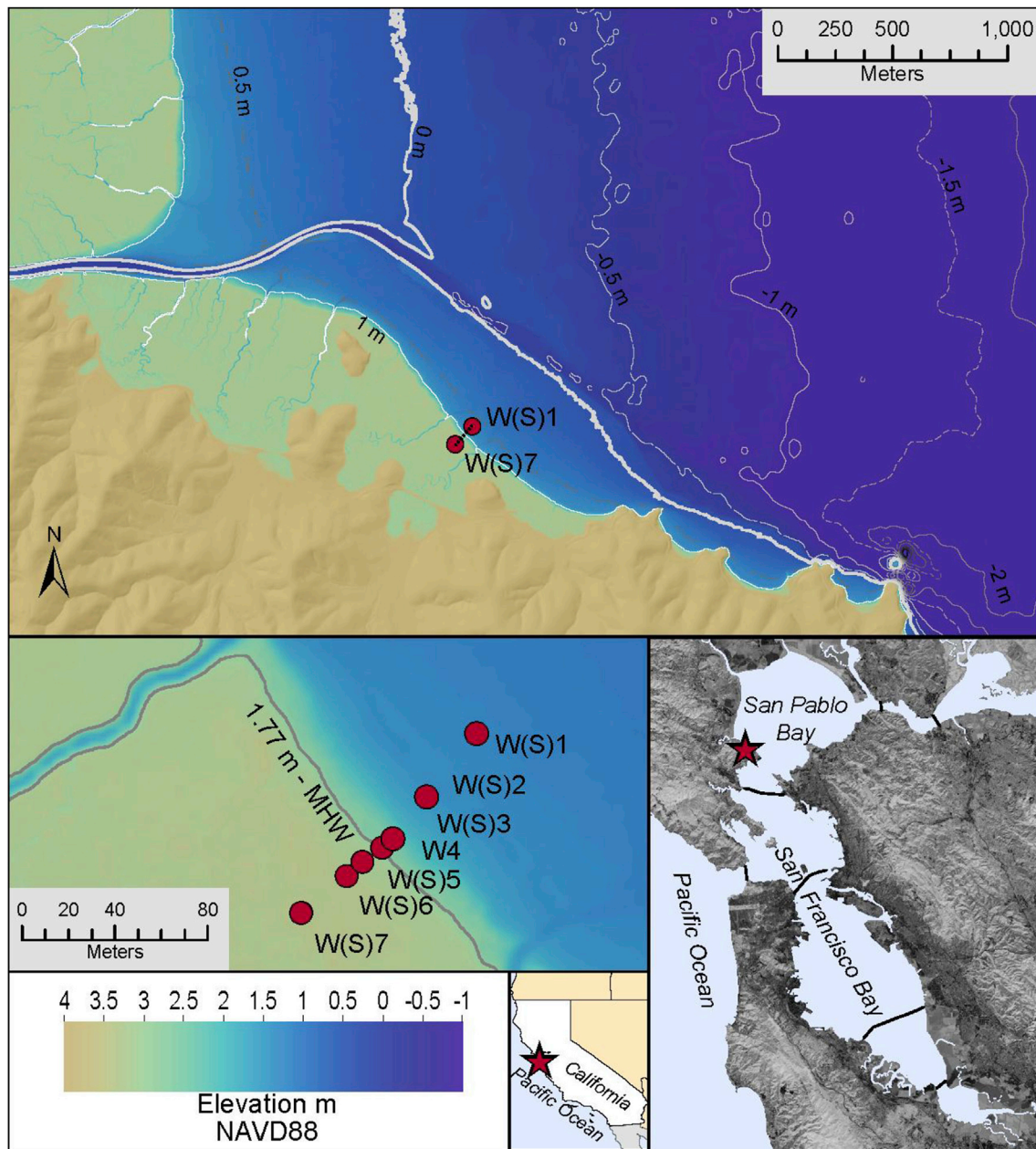


Fig. 1. Bathymetry of San Pablo Bay with the stations of the cross-shore transect. Inset in lower right shows San Pablo Bay and China Camp State Park (star) within the San Francisco Bay system.

2. Methods

2.1. Field site

San Pablo Bay is the northwestern extremity of the San Francisco Bay system. It is characterized by broad shallows with a deep channel along the southeastern edge that connects the Pacific Ocean to the ports and industries of the Sacramento-San Joaquin Delta (Fig. 1). The shores of San Pablo Bay contain about 80% of the remaining marshes of San Francisco Bay (Beagle et al., 2015). The Mediterranean climate in the region creates a strong seasonal signal; the winters are marked by episodic storms followed by periods of calm, while the summers are dry with consistent afternoon sea breeze (Cloern and Nichols, 1985). In the center of San Pablo Bay, the sea breeze generates significant wave heights of about 0.5 m, and storms can generate significant wave heights up to 0.8 m (Lacy and MacVean, 2016).

The study area is a 96.7 ha tidal salt marsh within China Camp State Park, a component of the San Francisco Bay National Estuarine Research Reserve (Takekawa et al., 2013; Ferner, 2012). The bayward portion of the salt marsh was created by sediment delivery from mining activities near the end of the 19th century and is characterized by nearly straight tidal creeks, while the landward portion is prehistoric and has a complex and sinuous channel network (Baye, 2012; Goman et al., 2008). This polyhaline to hyperhaline site has a semidiurnal tidal cycle with a mean tidal range of 1.3 m and a spring tidal range of 2 m (Callaway et al., 2012; Fagherazzi et al., 2004). Outside the marsh, there are extensive intertidal mudflats that extend into San Pablo Bay. These mudflats reduce incoming wave energy (Lacy and MacVean, 2016), and the marsh location shields it from southerly waves. Cores dated with ^{137}Cs show the site has been keeping pace with sea-level rise over the last half century with a vertical accretion rate of 0.63 cm/yr in the low marsh and 0.36 cm/yr in the mid marsh (Callaway et al., 2012). These accretion rates and vegetation patterns are considered indicative of a healthy marsh in this region.

The low marsh is characterized by a narrow fringe of *S. foliosa*, a zone that typically spans elevations of 0.4–1.1 m relative to mean low water (MLW = 0.37 m NAVD88) (Takekawa et al., 2013; Swanson et al., 2014). There are portions of San Pablo Bay without this fringing *S. foliosa* and other areas where it is up to 50 m wide (Baye, 2012). Baye (2012) observed that this zone width grows after calm winters, suggesting the zone width is controlled in part by storm activity. In the upper marsh (generally +1.3 m MLW), the dominant vegetation is *S. pacifica* (Baye, 2012; Takekawa et al., 2013). The transition zone contains both *S. foliosa* and *S. pacifica* and extends from approximately +0.7 to +1.3 m MLW (this study). The spring-neap cycle is important at this site, as the upper marsh is primarily inundated on high spring tides.

2.2. Field data collection

To capture differences in vegetation and wave conditions, we conducted two field campaigns. The first was in December 2014 and January 2015 (winter dataset), and the second was in May and June 2016 (summer dataset). Each campaign included a vegetation survey and deployment of instrumentation to measure wave evolution.

2.2.1. Vegetation surveys

Vegetation surveys were conducted on January 23, 2015, and June 6, 2016; both surveys occurred while instruments were deployed. One-meter quadrats were analyzed for percent cover of each vegetation species present, average canopy height, and maximum canopy height. A quarter-meter quadrat (0.0625 m^2) was then used for stem count and stem diameter measurements. Stem counts were done for *S. foliosa* but not for *S. pacifica*; *S. pacifica* has a high number of branching stems, making the number of stems connected to the ground not representative of the vegetation density. Instead, for *S. pacifica*, estimates were made of the solid volume fraction occupied by vegetation, ϕ . These estimates were made in the field and were based on visual inspection from three

researchers. The stem count was then back-calculated from ϕ assuming cylindrical stems and using the measured stem diameter. Destructive biomass sampling in the area from previous studies, as well as documented growth patterns of *S. pacifica*, indicate that the number of stems does not greatly change with the season (Mahall and Park, 1976). Therefore, the value that was estimated for summer was also used in winter. Photographs were taken of each quadrat at the time of the surveys.

Information on the vertical structure of vegetation is important to characterizing the drag but is not part of standard vegetation surveys. To gather more information on the distribution of drag elements, additional vegetation surveys were conducted on September 29, 2016 (at the site) and May 31, 2017 (section of the marsh adjacent to the study area). The length, width, and spacing along the stem of *S. foliosa* leaves were measured.

2.2.2. Wave attenuation measurements

We deployed instruments on a cross-shore transect (Fig. 2). This transect started on the mudflat 35 m outside of the start of vegetation and ended 75 m into the vegetation in the upper marsh. The stations were placed to mark changes in the dominant vegetation type, creating four zones: mudflat, *S. foliosa*-dominated, transition between *S. foliosa* and *S. pacifica* (transition zone), and *S. pacifica*-dominated. We measured the precise position and elevation of each instrument station using RTK-GPS; the GPS base station was located on an established benchmark 0.5 km away (precision of 0.02 m in the horizontal and 0.01 m in the vertical directions). Because the outer station on the mudflat was not accessible by foot, the elevation was taken from bathymetry data. There is a 1.4 m elevation gain from the first station to the last. We measured the topography of the transect on foot using Trimble R7 and R10 GNSS backpack-mounted receivers and taking readings approximately every 2 m along the transect at the time of the vegetation surveys.

Instrument deployments along the marsh transect spanned periods of perigean spring tides, the greatest inundation depths of the year. A timeline of deployments can be found in Fig. 3. For both the winter and summer, the stations bordering the mudflat were deployed longer than stations in the marsh. In winter, there were two separate marsh deployments. The first contained six instrument stations, and the second repeated the locations of the first with an additional station in the transition zone. In the summer, there was a single deployment that occupied approximately the same locations of the second winter deployment. During the summer deployment, one station (S4) had a battery failure and collected no data. Thus, the winter transition zone is resolved into two sections, and the summer contains one.

We deployed a high-frequency pressure sensor (6 or 8 Hz) at each instrument station. A “burst” of measurements were taken at 10 or 15 min intervals; each burst was 2048 measurements, which is approximately 5 min depending on the sampling frequency.

The elevation of the pressure sensors was measured when the sensors were installed. Stations bayward of the vegetation had sensors positioned 0.16–0.27 m above the bed, and stations in the vegetation were positioned less than 0.05 m from the bed. The pressure data was converted to water depth by assuming a constant water density, subtracting atmospheric pressure, and adding the elevation of the sensor above the bed. For the winter dataset, atmospheric pressure was measured at the site with a TWR-2050 pressure sensor, and for the summer dataset, measurements were obtained from the NOAA RCMC1 weather station (11.5 km from the site).

There is evidence that some instrument stations settled over time, particularly those outside of the vegetation. Adjustments were made to the depth measurements by examining the water-surface elevations over the course of the deployment. In both datasets, slight (<5 cm) adjustments were made to correct for vertical movement. In the winter, W2 drifted horizontally by approximately 10 m during the deployment; we corrected its position in our data.

Only data from inundated bursts were used for wave analysis, where

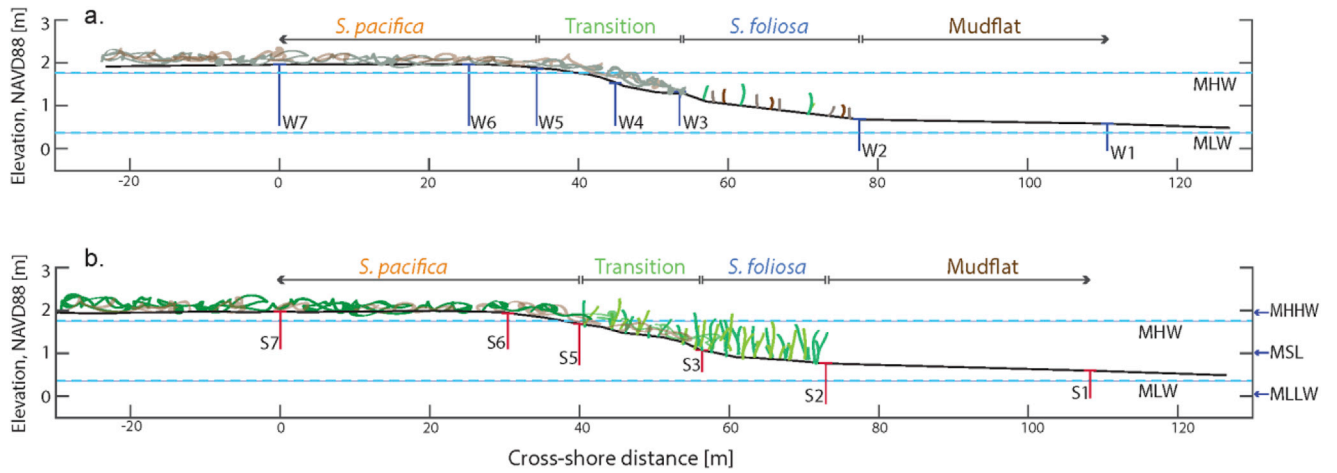


Fig. 2. Instrument locations and vegetation zones along the cross-shore transects for (a) winter and (b) summer deployments. Datums relative to NAVD88: MLLW = 0.06 m; MLW = 0.37 m; MSL = 1.01 m; MHW = 1.77 m; MHHW = 1.95 m (Goman et al., 2008). Sketch of vegetation depicts the general morphology and condition but is not an exact representation. Station S4 is not shown because the instrument did not collect data.

Winter 2014:



Summer 2016:



Fig. 3. Timeline of instrument deployments. Portions in purple and green are marsh stations and in brown are mudflat stations. The location of these stations is shown in Fig. 2. (For interpretation of the references to colour in this figure legend, the reader is referred to the Web version of this article.)

inundation is defined as the burst-mean depth being 2 cm above the height of the pressure sensor. Wave statistics, including root-mean-square wave height (H_{RMS}), and peak period (T_p), were calculated from the pressure frequency spectra following the methods of Wiberg and Sherwood (2008). The pressure timeseries from each burst had linear trends removed and were corrected for attenuation with depth below the water surface. We used a low-frequency cutoff of 0.2 Hz. The high frequency cutoff was calculated as follows for each burst:

$$f = \sqrt{\frac{g}{4\pi(h - h_s)}} \quad (1)$$

where h is the mean depth for the burst, and h_s is the height of the pressure sensor. This frequency defines the highest frequency that penetrates to the depth of the sensor. Bottom orbital velocity (u_B) was calculated from H_{RMS} and T_p . These calculations, as well as the high frequency cutoff, are based on linear wave theory. Wave attenuation was determined from simultaneous bursts from two adjacent stations when both had $H_{RMS} > 0.001$ m, which is 5 times greater than the resolution of the instrument.

2.3. Modeling wave attenuation

Vegetative resistance is commonly modeled as a drag force. Dalrymple et al. (1984) derived an expression for energy dissipation of monochromatic waves through a vegetated field, treating the vegetation elements as rigid cylinders. Mendez and Losada (2004) modified this expression for a random wave field. They also developed an analytical solution for monochromatic shallow-water waves on a sloped plane, where depth is not constant. Here, we started with this latter solution:

$$H_{RMS} = H_{0, RMS} K_s K_v \quad (2)$$

Where

$$K_s = \frac{h_0^{1/4}}{h^{1/4}} \quad (3)$$

$$K_v = \frac{1}{1 + 2 \frac{A_2}{m} H_{0, RMS} (K_s - 1)} \quad (4)$$

$$h = h_0 - mx \quad (5)$$

x is the distance between the two stations, and m is the bed slope. The '0' subscript indicates the offshore station. K_s is a shoaling coefficient (Green's law (Dean and Dalrymple, 1991)), which describes the increase in wave height due to the decrease in water depth, and K_v is the vegetative-dissipation coefficient. We then applied the modification for a random wavefield (Mendez and Losada, 2004), assuming a Rayleigh distribution of wave heights:

$$A_2 = \frac{2C_D N b_v \alpha_* 3\sqrt{\pi}}{3\pi} = \frac{C_D N b_v \alpha}{2\sqrt{\pi}} \quad (6)$$

b_v is the diameter of the vegetation stem, N is the number of vegetation stems in a square meter, α is the ratio of the vegetation height to the water depth (h_v/h), and C_D is the drag coefficient. Given our data, C_D is the only free parameter. Since the vegetation is in reality flexible, C_D is assumed to account for vegetation motion as part of the drag force. These expressions ignore nonlinear processes, such as wave reflection and interaction between stems. They were originally derived for submerged

vegetation but have been used for emergent conditions (Anderson and Smith, 2014). Two other models for calculating C_D were also explored (see Appendix for details). We found that Eq. (2) is preferable, as it is a conservative approach that incorporates the effects of bottom slope.

By linearizing the force acting on the vegetation, Kobayashi et al. (1993) showed the change in wave height can be approximated as an exponential decay:

$$\frac{H_{RMS}}{H_{0,RMS}} = e^{-k_i x} \quad (7)$$

where k_i is the exponential decay constant. This model assumes constant depth. Although our site has a non-zero bed slope, we used Eq. (7) to examine the bulk attenuation per unit distance for pairs of adjacent stations.

2.4. Modeling bed friction

Bed friction is another mechanism of wave dissipation. While it is not the focus of this study, it was calculated to judge its importance relative to vegetative drag. The bed friction coefficient, K_f , is defined as follows for a turbulent wave boundary layer along a rough, flat bottom (Dean and Dalrymple, 1991):

$$K_f = \left[1 + \frac{8f_w}{6\pi} \frac{k_p^2 H_{0,RMS}^x}{(2k_p h + \sinh(2k_p h)) \sinh(k_p h)} \right]^{-1} \quad (8)$$

where k_p is the wavenumber associated with peak period, and f_w is the wave friction factor. A common definition for f_w in rough flows is (Nielsen, 1992; Swart, 1974):

$$f_w = \exp \left[5.213 \left(\frac{k_b}{A} \right)^{0.194} - 5.977 \right] \quad (9)$$

where k_b is the roughness length scale, and $A = T_p u_B / 2\pi$ is the wave orbital amplitude. Lacy and MacVean (2016) validated the use of these expressions for San Pablo Bay mudflats.

3. Results

3.1. Vegetation characteristics

The vegetation surveys confirmed the strong seasonal signal in *S. foliosa* biomass and lack of one in *S. pacifica* biomass. Key features of these two vegetation species during both seasons are given in Table 1. The product of stem density and width (N^*b_v) is a direct input in our calculation of drag coefficients and is a measure of the width taken up by vegetation in the water column. In the winter, most *S. foliosa* leaves are lost, and the vegetation consists of shorter stems and stubble; whereas in the summer, *S. foliosa* is taller and has many leaves (Fig. 4a and b). To account for these leaves, the summer N^*b_v includes two leaf widths

(8 mm each), as our field data (details given in Section 2.2.1) showed on average two overlapping leaves at a given point along the stem. By contrast, *S. pacifica* retains much of its aboveground biomass in the winter months, and the height and structure between the seasons are similar (Fig. 4c and d). In the winter, much of the *S. pacifica* biomass has senesced, decreasing the diameter of the stems. Due to the narrower stem width the N^*b_v value decreases by a factor of two. The back-calculated stem count is high, but it includes all of the volume taken up by *S. pacifica* and is comparable to stem counts of *Salicornia europaea* ($N = 10,000$ (Ellison, 1987)). In the winter and summer, the N^*b_v values for *S. pacifica* are an order of magnitude larger than *S. foliosa*.

Seasonal changes also occur in the transition zone, which contains a combination of *S. foliosa* and *S. pacifica*. The parameters used for the transition zone are a weighted average of the values from the *S. foliosa* and *S. pacifica* zones. These averages were weighted by the percent coverage of the two species from observations in the field. The percent coverages are different for the two segments within the winter transition zone. The second segment, or transition zone 2, is mainly *S. pacifica*, but for our analysis we classify it as transition if the zone contained any amount of both species.

3.2. Tidal and wave conditions

The wave conditions during the study were typical of the San Francisco Bay system. The winter deployment captured periods of calm (e.g. January 21 in Fig. 5b) with sporadic storms (e.g. January 22 in Fig. 5b), and the summer had a consistent generation of waves from the afternoon sea breeze (Fig. 5e). The marsh platform was inundated more frequently during the summer deployment, but because the summer tides are not as energetic, the marsh was inundated to a greater depth in the winter. Larger waves were observed at the marsh edge during the winter deployment with a maximum H_{RMS} of 0.27 m versus a maximum of 0.12 m in the summer. Ninety-six percent of all waves just outside of the vegetation (at W(S)2) were classified as shallow or intermediate ($h/L_\infty < 1/20$ where $L_\infty = (g/2\pi)T_p^2$ deep-water wavelength). Typical peak period was 1.8 s in the summer and 2.1 s in the winter. No waves included in our analysis met the wave-breaking criteria ($H_{RMS} > 0.7h$); the wave heights were less than $0.6h$ in the winter and $0.3h$ in the summer.

3.3. Evolution of wave height

Wave heights decreased as waves moved onshore across the marsh. As seen in Fig. 6, some waves grew in height across the mudflat and *S. foliosa* zones due to shoaling, local wave generation, and/or wave interactions. No wave growth was observed across the transition and *S. pacifica* zones in either season. Complete attenuation was observed approximately 75 m into the vegetated marsh, as no waves greater than 0.001 m were recorded at the farthest landward station in either season (W(S)7). The mean percent reduction from W(S)2 to W(S)6, a distance of 51.3 m in winter and 42.6 m in summer, was $89 \pm 7\%$ and $86 \pm 6\%$ (\pm std %) respectively.

Table 1

Vegetation parameters from summer and winter deployments: b_v = stem width, N = number of stems per m^2 , ϕ = solid volume fraction of vegetation, h_v = vegetation height. Measured in the field unless otherwise noted.

		b_v (m)	N (m^{-2})	ϕ	% <i>S. foliosa</i>	% <i>S. pacifica</i>	h_v (m)	$h_{v,max}$ (m)	N^*b_v (m^{-1})
Summer	<i>S. foliosa</i>	0.0047	440	–	–	–	0.48	0.75	9.5 ^a
	Transition	–	–	–	70	17	–	–	32.1
	<i>S. pacifica</i>	0.0034	4.4E+04 ^b	0.4 ^c	–	–	0.25	0.50	150
Winter	<i>S. foliosa</i>	0.0027	312	–	–	–	0.16	0.35	0.8
	Transition 1	–	–	–	20	15	–	–	13.4
	Transition 2	–	–	–	5	55	–	–	48.5
	<i>S. pacifica</i>	0.002	4.4E+04 ^b	–	–	–	0.22	0.50	88.3

^a Includes stem width and width of two leaves (8 mm each).

^b Back-calculated from ϕ assuming cylindrical stems.

^c Estimated by visual inspection in the field.

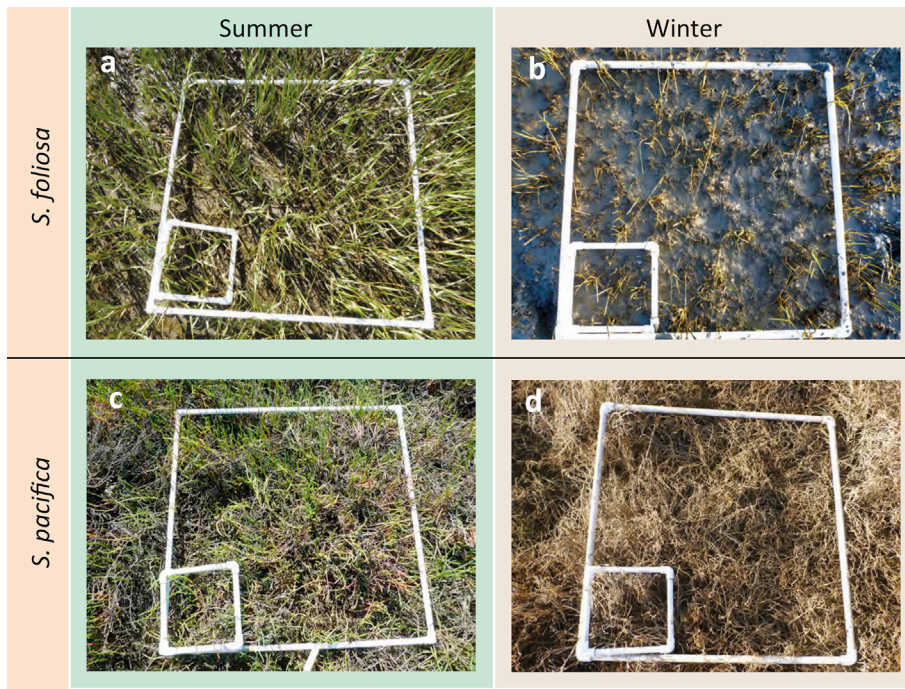


Fig. 4. Photographs of example vegetation quadrats from winter (b, d) and summer (a, c).

There was a total of 4504 attenuation measurements in the winter and 1858 in the summer (detailed in Table 2). These are not the numbers of bursts containing waves, but rather, the number of occurrences when simultaneous bursts from adjacent stations had waves, allowing the tracking of wave height.

3.3.1. Exponential decay constant

The degree of wave attenuation varied between the vegetation zones. The decay constants increase by approximately an order of magnitude with each zone from the mudflat into the marsh (Fig. 7). Across the mudflat and *S. foliosa* zone, the k_i -values are on the order of 10^{-3} , while the transition and *S. pacifica* zones values are on the order of 10^{-2} and 10^{-1} respectively. Based on these k_i -values, at a water depth of 0.4 m in each zone, 115 m of mudflat would be needed to achieve a 50% reduction in wave height, versus 6 m of *S. pacifica*. For the depths observed, the *S. pacifica* was the most effective at reducing wave heights.

3.3.2. Evolution of wave energy spectra

Spectra seen in Fig. 8a–d are an average of all bursts with wave heights between 0.02 and 0.04 m and peak wave periods between 2 and 3 s. On the lower side of the wave envelope up to the peak frequency, f_p , the wave energy is largely unchanged from the station farthest offshore, W(S)1, to W4 in the winter and S5 in the summer (Fig. 8a–b). Progressing landward past these stations, the energy is attenuated.

At frequencies greater than f_p , there is more dynamic behavior. In the winter, the peak broadens in the *S. foliosa* and first transition zones. The transfer of energy to higher frequencies is evidence of the development of a harmonic, which has been observed elsewhere (Herbers et al., 2003; Young and Babanin, 2006). In summer, there is much less change in energy, although the peak does broaden slightly across the transition zone (S3 to S5). Isolating the stations bordering the *S. foliosa* zone, the seasonal difference becomes more apparent (Fig. 8c–d). There is a difference of up to two orders of magnitude between W2 and W3, which is not seen between S2 and S3. It is likely the denser vegetation in the summer counteracts this energy growth.

Similar to the lower frequencies, the energy is attenuated in the *S. pacifica* zone, and there is no detectable wave energy past W(S)6. Some of these spectra contain noise amplification at high frequencies (i.e. W(S)

5 and W(S)6 > 1 Hz); these increases in wave energy should be disregarded.

3.3.3. Drag coefficient, C_D

Drag coefficients allow us to isolate the attenuation due to vegetation. Since vegetation, wave, and topography parameters were measured, C_D could be directly solved. Each zone of the transect had unique vegetation parameters (Table 1); therefore, a separate C_D was calculated for each zone. The equations used (Eqs. (2)–(6)) are for random, shallow waves along a sloping bottom. Not all waves measured were classified as shallow, but we relaxed this criteria and included all waves in the analysis.

The dependence on wave energy is typically represented by expressing C_D as a function of Reynolds number (Re) or Keulegan–Carpenter number ($KC = u_b T_p / b_v$). Here, we found a better fit with Re . The wave Reynolds number is defined as $Re = u_b b_v / \nu$, where ν is kinematic viscosity and u_b is the orbital velocity at the top of the vegetation. The orbital velocity at the top of the vegetation was used because it is the maximum velocity that interacts with the vegetation and is the most consistent value for comparison between studies.

The C_D values were then binned by Re . The general trend is a decrease in C_D with an increase in Re (Fig. 9). The data was binned such that each bin contains the same number of data points. This binning scheme causes some bins to cover a wider range of Re than others. The winter *S. pacifica* has the highest overall C_D values but experienced relatively low Re .

The results from winter *S. foliosa* were not described well using Eq. (2); the interquartile range at low Re spanned three orders of magnitude. The wave attenuation for this zone was comparable to that for the unvegetated mudflat and was better described by bed friction, presented in Section 2.4, and shoaling. The winter *S. foliosa* results best fit the model:

$$H_{RMS} = H_{0,RMS} K_f K_s \quad (10)$$

The roughness length scale, k_b , within the K_f term was used as a fitting parameter, rather than being based on physical measurements of the vegetation. Using the best fit, we determined k_b to be 0.04 m. This model and k_b value also described the summer *S. foliosa* data well. However, the vegetation dissipation model (Eq. (2)) was preferred for this zone since it

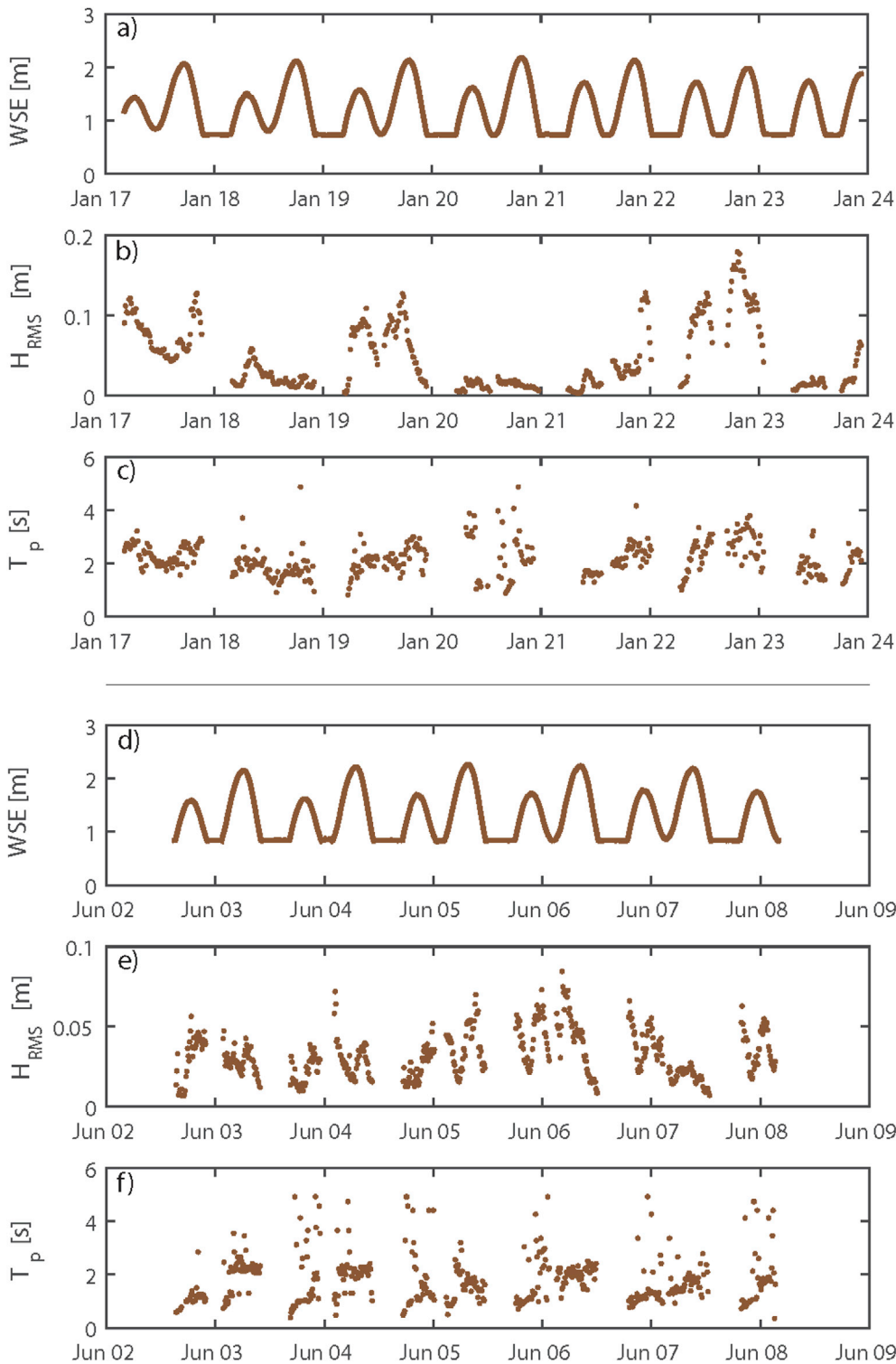


Fig. 5. Example hydrodynamic characteristics at W1 (a–c) in winter and S1 (d–f) in summer. WSE = water surface elevation; H_{RMS} = root mean square of wave height; T_p = peak period.

is more physically meaningful.

To assess the importance of bed friction across the transect, C_D values were calculated with and without bed friction using the following:

$$H_{RMS} = H_{0,RMS} K_f K_s K_v \quad (11)$$

Eq. (11) was applied to all of the zones with a k_b of 0.01 m, which was previously measured in the vicinity of our study site (Lacy and MacVean, 2016). Inclusion of this term caused a decrease in C_D but was deemed negligible. See the Appendix for details.

4. Discussion

4.1. Variations within China camp salt marsh

Measurements of wave attenuation through the *S. foliosa* and into the *S. pacifica* zones show that these species attenuate wave heights to different degrees. The exponential decay constants for *S. pacifica* are two orders of magnitude greater than those for *S. foliosa*, meaning greater attenuation occurred across the *S. pacifica* zone (Fig. 7). The vegetative

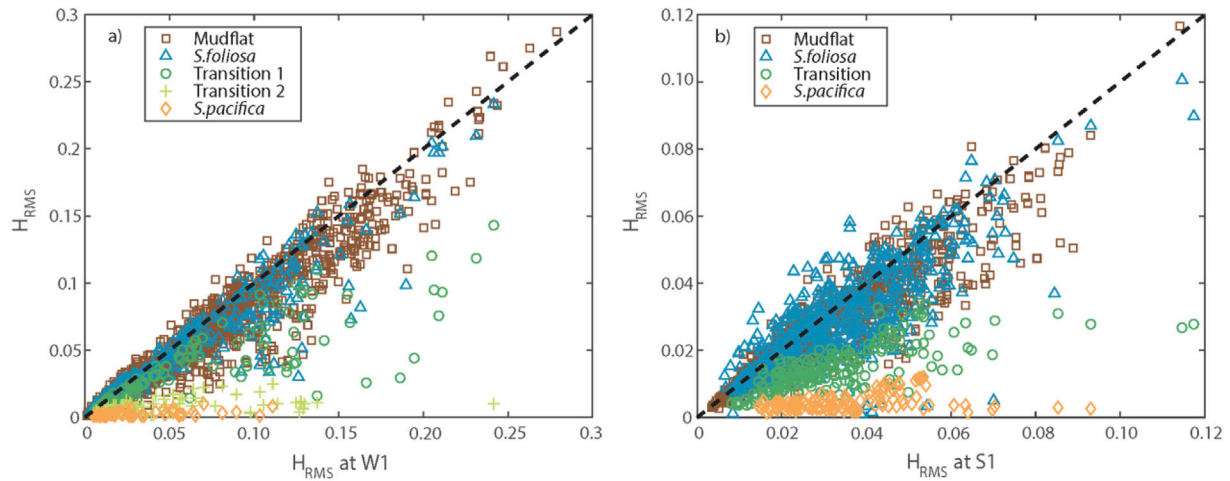


Fig. 6. H_{RMS} at W(S)1 versus the H_{RMS} recorded at the end of each respective zone for (a) winter and (b) summer. Note the different axes scales. The dashed line indicates 1:1 correspondence.

Table 2

Number of wave attenuation measurements in winter (W1-W7) and summer (S1-S7).

Station ID	Category	No. of wave attenuation measurements
W1 to W2	Mudflat	2887
W2 to W3	<i>S. foliosa</i>	793
W3 to W4	Transition 1	529
W4 to W5	Transition 2	140
W5 to W6	<i>S. pacifica</i>	155
W6 to W7	<i>S. pacifica</i>	0
Total		4504
S1 to S2	Mudflat	1303
S2 to S3	<i>S. foliosa</i>	214
S3 to S5	Transition	215
S5 to S6	<i>S. pacifica</i>	126
S6 to S7	<i>S. pacifica</i>	0
Total		1858

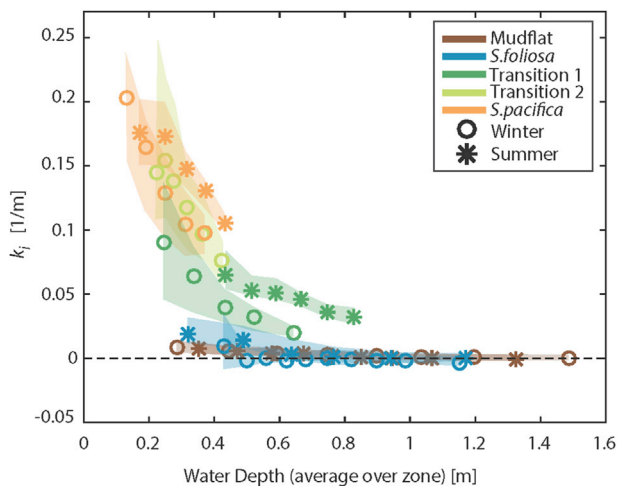


Fig. 7. Wave height exponential decay constants binned by depth. Shaded regions are the interquartile range, and markers are at the bin median.

drag modeling, however, shows the two species have similar C_D values (Fig. 9). Thus, differences in attenuation are due to slope or vegetation density, not single stem morphology. For example, this result indicates that under the same hydrodynamic conditions, 1-cm wide section of *S. foliosa* provides a similar drag as 1-cm of *S. pacifica*.

Yet due to their presence in different elevations of the marsh, these species rarely experience the same hydrodynamic conditions. The maximum depth at W(S)6, in the *S. pacifica* zone, was 0.32 m in the summer and 0.34 m in the winter, meaning α (the ratio of vegetation height to water depth) had a minimum value of 0.67. *S. foliosa*, occupying a lower elevation in the marsh, was inundated to a greater depth and had minimum values of α of 0.33 in the summer and 0.10 in the winter.

The seasonal signal in wave attenuation is dominated by the changes in frontal area of the vegetation. Möller and Spencer (2002) documented seasonal changes in marshes on the Dengie Peninsula in England and found greater attenuation in summer months when more biomass was present. It is interesting that the degree of attenuation across the *S. foliosa* zone does not change much between summer and winter, despite the dramatic change in vegetation density and height (Fig. 7). One possible explanation is a seasonal shift in the mechanism of wave generation. The summer sea breeze may cause more local wave generation or re-generation that leads to increased wave propagation through the *S. foliosa* zone.

The exponential decay coefficients can be used to predict wave height evolution across the marsh, shown in Fig. 10 for a given set of offshore wave height and depth conditions. Differences between the seasons occur across the mudflat, *S. foliosa*, and transition zones. These different states of wave energy likely affect the local sediment dynamics, with increased energy in the winter leading to more sediment resuspension than in the summer. Since complete attenuation is reached at similar distances regardless of season, these differences do not greatly influence the final outcome. Many of San Francisco Bay's marshes do not have fringing *S. foliosa* and have vegetation more similar to the winter conditions at the study site year-round. Our results imply that these marshes are still effective in attenuating wave energy but may have different sediment delivery dynamics.

4.2. Dependence on relative depth

A dependence on water depth can be seen in both the decay constants and drag coefficients. Our findings demonstrate the expected result: there is greater attenuation when vegetation is emergent, and the drag force acts on the entire water column, than when the vegetation is submerged. This behavior is most visible across the *S. foliosa* zone (Fig. 11). There is a marked decrease in the decay coefficient when the water level at the upland end of the zone is at or above the vegetation. In the summer, the k_t -value decreases by an order of magnitude at this point (Fig. 11 depths past solid vertical line), and in the winter, most bin medians become negative, indicating wave growth (Fig. 11 depths past dotted vertical line). Even for the short *S. foliosa* stems, it makes a difference if they are

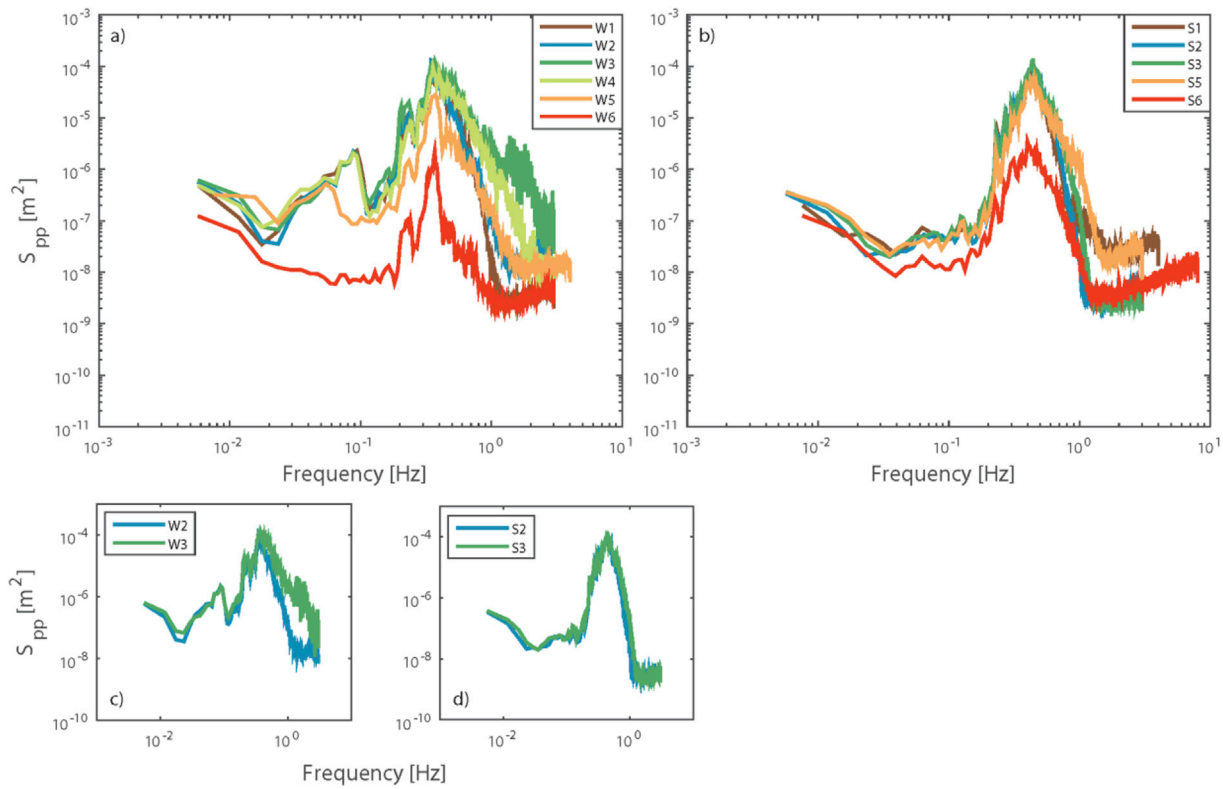


Fig. 8. Wave energy spectrum for bursts with wave height $0.02 < H_{RMS} < 0.04$ m and wave period $2 < T_p < 3$ s; a) All winter zones, $n = 16$ bursts; b) All summer zones, $n = 9$ bursts; c) Winter *S. foliosa* zone; d) Summer *S. foliosa* zone.

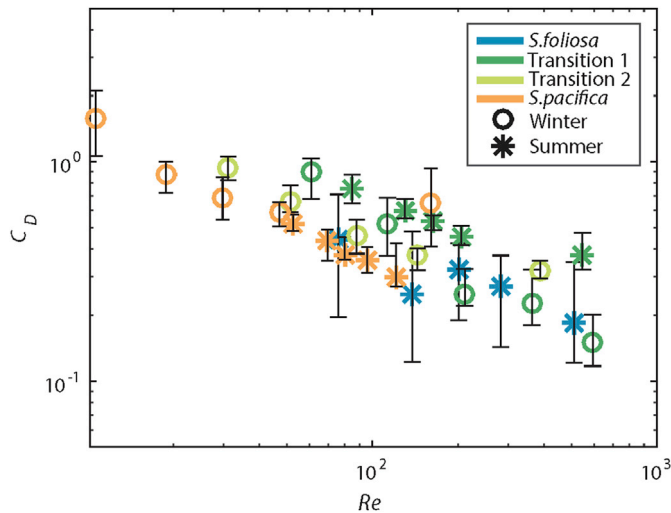


Fig. 9. C_D as a function of Re . Error bars show interquartile range.

deeply submerged. This result agrees with findings of Augustin et al. (2009), who studied wave attenuation in a laboratory under emergent and near-emergent conditions. With emergent vegetation, the wave attenuation was 50%–200% greater per wavelength (Augustin et al., 2009).

The vegetative drag model accounts for the height of the vegetation relative to the water depth via the α parameter (Eq. (6)); therefore, C_D should not be a function of α . Yet α can change with vegetation motion, and this motion is not in the model (Méndez et al., 1999). Möller et al. (2014) measured the change in plant posture with varying wave conditions and found that more attenuation occurred when stems were more upright. We examined the summer *S. foliosa* results as a function of α

(Fig. 12) and found greater drag coefficients when the vegetation was emergent ($\alpha \geq 1$) and presumably upright. We did not find this trend with α for *S. pacifica*, likely because the morphology of *S. pacifica* prevents the stems from greatly changing with depth conditions. Augustin et al. (2009) did not find a large difference between the C_D values of rigid cylinders and flexible material. However, the flexible material did not bend past 20° from vertical, suggesting it is only beyond this point that the stem bending affects the drag. The attenuation in the summer *S. foliosa* zone decreases with greater submergence both because less of the water column is influenced by vegetative drag and because stem bending is greater.

The vegetation heights reported here are an average measured visually in the field, and they do not account for spatial variability in the α values for individual plants. This variability occurs in most field studies, as vegetation is not typically uniform. Furthermore, a sloped marsh profile means that the water depth, and thereby the α value, varies in the cross-shore direction. Studies often point to α as a central parameter for determining the effectiveness of a salt marsh at attenuating waves (e.g. Narayan et al., 2016a), so it is important to understand these local variations and sources of uncertainty when interpreting or applying wave attenuation results.

4.3. Variations among vegetation species

Researchers have measured drag coefficients for a range of vegetative and hydrodynamic conditions both in the lab and in the field. Constant C_D values have been found to overestimate attenuation because C_D decreases with increasing wave energy (Pinsky et al., 2013). Other studies (e.g. Möller et al., 2014; Pinsky et al., 2013; Anderson and Smith, 2014; Kobayashi et al., 1993; Jadhav et al., 2013) have found the relationship $C_D = a + (b/Re)^c$ to describe results well. We applied that fit to the binned data for each zone type (with the exception of winter *S. foliosa*). Fig. 13 shows this empirical relationship between C_D and Re for selected studies alongside the results of this study. The coefficients for our

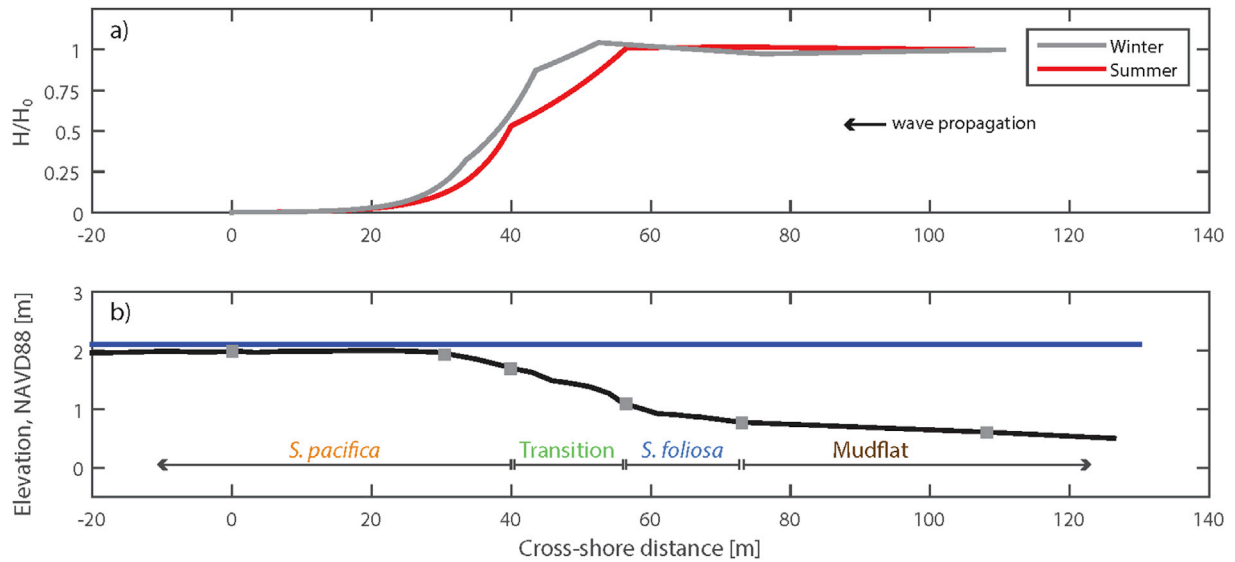


Fig. 10. a) Predicted wave attenuation for with a depth of 1.5 m at W(S)1 for summer and winter. Predictions are made from the exponential decay constants for each zone of marsh. b) Cross-shore summer bathymetry and water level. Stations are marked by squares.

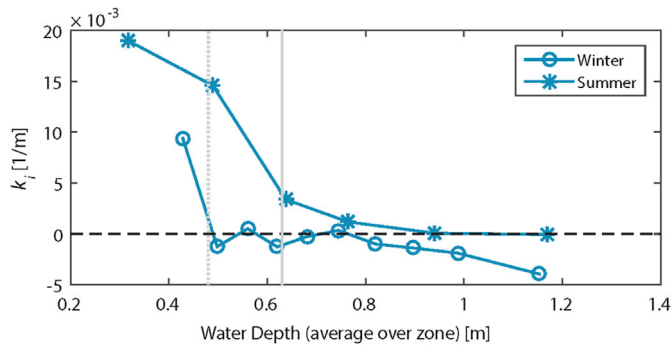


Fig. 11. Wave height exponential decay constants for the *S. foliosa* zone in winter and summer. Vertical gray lines indicate the transition from emergent vegetation to submerged in winter (dotted line) and summer (solid line).

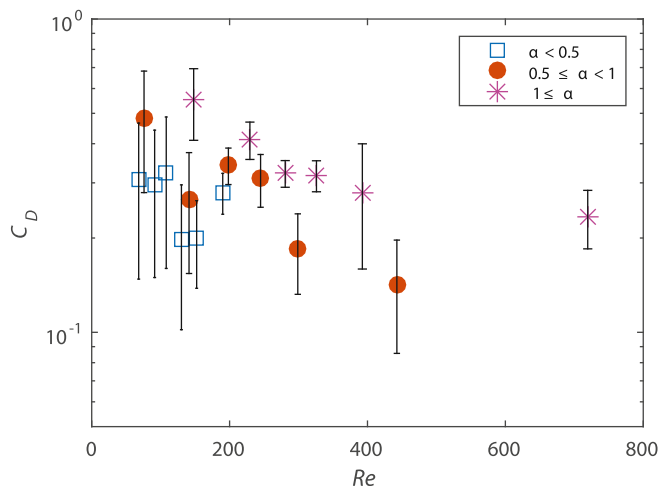


Fig. 12. C_D as a function of Re for summer *S. foliosa*. Symbols show different values of α ($\alpha = h_v/h$). For $\alpha > 1$, vegetation is emergent, and for $\alpha \leq 1$, vegetation is submerged. Error bars are standard error.

empirical fits as well as those of other authors are given in the Appendix. The results are applicable over the range of Re measured; hence the

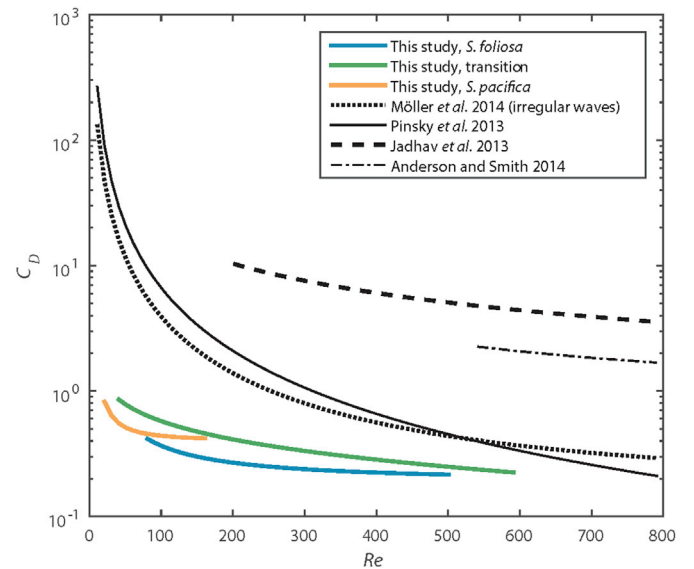


Fig. 13. Relationship between C_D and Re ($C_D = a + (b/Re)^c$) for four published studies along with this study. The setup and vegetation used in each study are as follows: Möller et al. (Möller et al., 2014), laboratory with real vegetation (primarily *Elymus athericus* and *Puccinellia maritima*); Pinsky et al. (2013), combination of the results from 14 marsh attenuation studies with varying vegetation species; Jadhav et al. (Jadhav et al., 2013), field with *S. alterniflora*; Anderson and Smith (Anderson and Smith, 2014), laboratory with polyolefin tubing mimicking *S. alterniflora*. Note the results from this study are shown over the range of the binned data, not the full range of Re observed.

functions are only shown where they overlap the range of Re measured in this study ($Re < 800$). This requirement limited the number of comparable studies, as the conditions that we observed here were less energetic than many others.

For a given Re , the C_D values vary by two orders of magnitude (Fig. 13). The two studies that focus on *S. alterniflora*, Anderson and Smith (2014) (lab study using polyolefin tubing) and Jadhav et al. (2013) (field study), exhibit the greatest C_D values. These results are followed by Pinsky et al. (2013), which is a combination of the results from 14 marsh attenuation studies with varying vegetation species, and Möller et al. (2014), who used real vegetation, primarily *Elymus athericus* and

Puccinellia maritima, in a laboratory flume.

It is likely that material differences between these species drive the differences in C_D . For example, stiffer plants may exert more drag, though the existing data is both noisy and seems to point in the opposite direction. Published values of Young's modulus are greater for *E. athericus* (2696.3 ± 1963.8 MPa (Möller et al., 2014)) than for *S. alterniflora* (1410 ± 710 MPa (Feagin et al., 2011)).

We can also use the measured exponential decay constants to compare *S. foliosa* and *S. alterniflora*. Ysebaert et al. (2011) and Paquier et al. (2016) measured attenuation across *S. alterniflora* in the Yangtze estuary and Chesapeake Bay, respectively. They reported exponential decay constants that vary from 0.02 to 0.12 m^{-1} with increasing depth, which correspond to much greater attenuation than the k_t -values for *S. foliosa* measured here. These different values support the idea that the structural differences between the *Spartina* species produce the differences in C_D values. San Francisco Bay contains non-native *Spartina* species, including *S. alterniflora*. While the coverage of non-native *Spartina* has decreased by 96% in recent years (Rohmer et al., 2015), the difference between our results and those for *S. alterniflora* suggests that attention should be given to the species present when modeling wave attenuation in a specific area.

Since *S. alterniflora* is well-studied and widespread in salt marshes, it is worthwhile to compare the wave attenuation in the transition zone and *S. pacifica* zone to that of *S. alterniflora*. At our study site, the attenuation rates increased greatly moving into the transition zone and are comparable to the sparse ($N=97$ (Paquier et al., 2016)) *S. alterniflora*. The *S. pacifica*-zone rates were the highest measured, exceeding those of dense ($N=334$ (Ysebaert et al., 2011)) *S. alterniflora*. The higher drag coefficients indicate that on a per width basis, *S. alterniflora* exerts a greater drag than *S. pacifica*. However due to the high amount of *S. pacifica* biomass, a larger portion of the water column is occupied by vegetation, and *S. pacifica* attenuates wave energy in shorter distances compared to *S. alterniflora*. Recall the conditions studied cover a limited range of α -values for this zone ($\alpha > 0.67$). Deeply submerged conditions should be tested to better understand the attenuation capacity of *S. pacifica*. Since it is typically found in the high marsh ($+1.3$ m MLW), encountering deeply submerged conditions is rare at this site.

4.4. Sources of uncertainty

The comparatively low C_D values in our study may be due in part to differences in what was included in the vegetation parameters. The stem counts for *S. pacifica* were back-calculated from estimates of the volume occupied by vegetation and therefore, include all of the biomass encountered by incoming waters. A similar approach was used for the *S. foliosa*, and the leaves in addition to the stems were included in the N^*b_v parameter. If we instead restrict N^*b_v to the rigid stem alone, it would decrease by a factor of five causing the C_D values to increase by the same factor. The C_D values become greater because the observed attenuation is then attributed to a smaller area of vegetation.

Similarly, another source of uncertainty arises from the initial assumption of uniform vegetation characteristics. Our vegetation surveys revealed heterogeneity even within monocultures. We used the smallest and largest measurements of N^*b_v in the summer *S. foliosa* zone to show the sensitivity of C_D to vegetation parameters (Fig. 14). Allowing N^*b_v to range from 3.5 (stem width = 3 mm; leaf width = 3 mm) to 13.8 (stem width = 8 mm; leaf width = 10 mm) produced an order of magnitude difference in C_D at low Re and shifted the results to larger range of Re values.

4.5. Implicit vs. explicit representation of vegetation

Wave dissipation over the *S. foliosa* zone was well described with a bottom friction model by increasing the roughness length scale, k_b , to 0.04 m. Other studies, primarily those of seagrasses, have also used this approach to implicitly represent dissipation due to vegetation; k_b -values

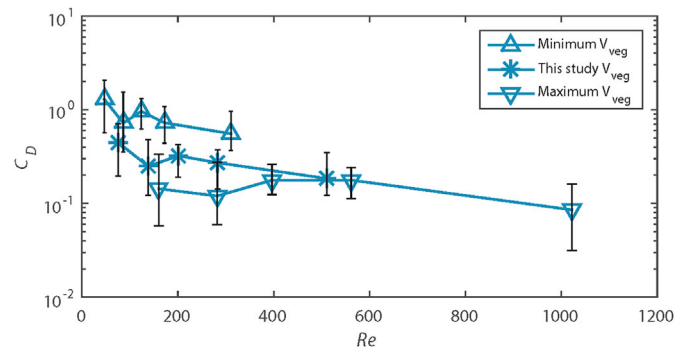


Fig. 14. Relationship between C_D and Re ($C_D = a + (b/Re)^c$) for *S. foliosa*. Minimum volume of vegetation (V_{veg}) uses the smallest vegetation parameters measured in the field, and maximum V_{veg} uses the largest. Error bars are interquartile range.

ranging from 0.03 m (*Zostera marina* (Nowacki et al., 2017)) to 0.4 m (*Posidonia oceanica* (Infantes et al., 2012)) have been found to agree well with attenuation observations. The stem densities for those studies tended to be much higher ($N = 600$ – 4600); although perhaps the increased rigidity of *S. foliosa* compensates for the decreased density, making the apparent roughness similar. Nowacki et al. (2017) showed that an implicit formulation, following the methods of Collins (1972) with $C_f = 0.4$, was able to out-perform the explicit representation of vegetation following the methods of Mendez and Losada (2004). The explicit representation may be viewed as advantageous because it is a more mechanistic approach and can be implemented using standard vegetation measurements. It is not yet clear how to estimate the equivalent roughness length scale, which can vary over an order of magnitude. However, as seen with the winter *S. foliosa* characterized in our study, not all vegetation data is best modeled with the explicit formulation.

5. Conclusions

We measured wave height evolution in the summer and the winter across a tidal salt marsh in San Francisco Bay. The marsh vegetation dissipated wave energy, and complete attenuation was reached less than 75 m into the vegetation. Attenuation rates followed seasonal shifts in biomass. Wave attenuation was greater when more vegetation occupied the water column because of shallower inundation, denser vegetation, or both. The greatest rates of attenuation occurred in the *S. pacifica* zone, which did not experience high levels of inundation. As a low-marsh species, *S. foliosa* was exposed to greater wave heights and water levels, and net wave growth occurred across this zone when the plants were deeply submerged ($\alpha < 0.3$ in the winter and $\alpha < 0.4$ in the summer). Under similar conditions, published attenuation rates for *S. alterniflora* are greater than and less than those found here for *S. foliosa* and *S. pacifica*, respectively.

We presented drag coefficients as a function of Re and exponential decay constants as a function of water depth. These relationships can be used to predict wave height in locations with vegetation and hydrodynamics similar to our study site. Using the exponential decay constants requires the same amount of vegetation present, as well as the same slope, but they can be used as a first-order approximation, especially for *S. pacifica* which occupies a narrow range of elevations. Use of the C_D values requires more information on the hydrodynamics (i.e. Re) and vegetation parameters (i.e. stem diameter and density). The application of this model to *S. pacifica* would be greatly improved with a standardized method for measuring the volume occupied by the vegetation, ideally one that is nondestructive.

Predictive models have been run for future scenarios of sea-level rise for China Camp Salt Marsh with varying levels of suspended sediment. Results from both the Wetland Accretion Rate Model of Ecosystem

Resilience (WARMER) and Marsh Equilibrium Model (MEM) show that by 2110, the whole marsh could be converted to mudflat (Swanson et al., 2014; Schile et al., 2014). At a constant depth of 0.5 m, a 0.20 m wave would propagate well over 0.5 km across mudflat before dissipating. Along some shorelines, such elevated wave heights could then have an impact on the surrounding seawalls and levees. Datasets, like the one from this study, can help inform these future scenarios and be used to develop best practices for coastal land management.

Acknowledgements

The authors would like to thank Rachel Allen, Joanne Ferreira, Jenny White, Tim Elfers, Pete DalFerro, Cordell Johnson, and Josh Logan for supporting field operations; Anna Deck for support in conducting vegetation surveys; Theresa Fregoso for creating Fig. 1. Daniel Nowacki (USGS) and two anonymous reviewers provided comments that

improved the manuscript. This research was made possible in part by funding from the US Geological Survey Coastal and Marine Geology Program, by a National Science Foundation Graduate Research Fellowship (DGE-1106400) and internship provided through the Graduate Research Internship Program (GRIP), and by an award under the Coastal Zone Management Act, administered by NOAA's Office for Coastal Management, to San Francisco State University. Any findings and conclusions or recommendations expressed in this material are those of the authors and do not necessarily reflect the views of the National Science Foundation. Coordination of GRIP at USGS is through the Youth and Education in Science programs within the Office of Science Quality and Integrity.

Hydrodynamic and vegetation data are available on Science Base (Lacy et al., 2017), and MATLAB codes to process the data are available by request from MRFM (madeline@berkeley.edu).

Appendix A. Supplementary data

Supplementary data related to this article can be found at <https://doi.org/10.1016/j.coastaleng.2018.02.001>.

Appendix

A1. Models for calculating C_D

To determine the drag coefficient, we follow the derivation of Mendez and Losada (2004) for energy dissipation due to vegetation. They present derivations for random waves along a flat-bottom, as well as monochromatic, shallow water waves along a sloping bottom. Here, we combine these derivations to show three ways to analytically determine the drag coefficient for vegetation: Case 1 - Random waves along a flat bottom; Case 2 - Random shallow water waves along a flat bottom; Case 3 - Random shallow water waves along a sloping bottom. Case 1 is derived in Section 2.3 of Mendez and Losada (2004), and Case 2 is a simplification of the Case 1 result for shallow water waves. Case 3 is shown below.

Wave energy is dissipated due to vegetative drag:

$$\frac{\partial E c_g}{\partial x} = -\varepsilon_v \quad (A1)$$

Where E is the energy density ($\frac{1}{8}\rho g H_{RMS}^2$) and c_g is group velocity, which can be approximated as \sqrt{gh} for shallow conditions. H_{RMS} is the root mean square of the wave height for a given burst, and g is the gravitational constant. For a random wave field that follows a Rayleigh distribution, the following are true:

$$\int_0^\infty H^3 p(H) dH = \frac{3\sqrt{\pi}}{4} H_{RMS}^3 \quad (A2)$$

And

$$H_{RMS}^2 = \int_0^\infty H^2 p(H) dH \quad (A3)$$

H is the time-varying wave height from which H_{RMS} originates. We can write the dissipation due to vegetative drag as:

$$-\varepsilon_v = -\left(\frac{2}{3\pi}\right) \rho C_D b_v N \left(\frac{g k_p}{2\sigma_p}\right)^3 \frac{\sinh^3 k_p a h + 3 \sinh k_p a h}{3 k_p \cosh^3 k_p h} \frac{3\sqrt{\pi}}{4} H_{RMS}^3 = -\frac{\rho C_D b_v N g^{3/2} \alpha}{16\sqrt{\pi} h^{1/2}} H_{RMS}^3 \quad (A4)$$

Where the expression farthest to the right has been simplified for shallow conditions. Here, b_v is the diameter of the vegetation stem (m), N is the number of vegetation stems in a square meter (m^{-2}), α is the ratio of the water depth to the vegetation height (h_v/h), k_p is the wavenumber associated with the peak period, σ_p is the wave frequency associated with the peak period, and C_D is the coefficient of drag. Substituting Eq. (A3) and Eq. (A5) into Eq. (A1) gives:

$$\frac{1}{8} \rho g^{2/3} \frac{\partial (H_{RMS}^2 h^{1/2})}{\partial x} = -\frac{\rho C_D b_v N g^{3/2} \alpha}{16\sqrt{\pi} h^{1/2}} H_{RMS}^3 \quad (A5)$$

Because h varies with distance x , it cannot be pulled out of the derivative. Rearranging, this gives:

$$\frac{\partial (H_{RMS}^2 h^{1/2})}{\partial x} = -A_2 \frac{H_{RMS}^3}{h^{1/2}} \quad (A6)$$

where

$$A_2 = \frac{2C_D b_v N \alpha}{3\pi} \frac{3\sqrt{\pi}}{4} = \frac{C_D b_v N \alpha}{2\sqrt{\pi}} \quad (\text{A7})$$

Solving Eq. (A6) with boundary conditions ($H_{RMS} = H_{0, RMS}$ at x_0) gives:

$$H_{RMS} = H_{0, RMS} K_s K_v \quad (\text{A8})$$

Where

$$K_s = \frac{h_o^{1/4}}{h^{1/4}} \quad (\text{A9})$$

$$K_v = \frac{1}{1 + 2 \frac{A_2}{m} H_{0, RMS} (K_s - 1)} \quad (\text{A10})$$

and

$$h = h_o - mx \quad (\text{A11})$$

This result is identical to that of Mendez and Losada (2004) for shallow water waves with monochromatic wave height over a sloping beach with the exception of the constants in the A_2 term. K_v is the vegetation damping coefficient, and K_s is the coefficient of shoaling. Table A1 gives the resulting equations for each case.

Table A1

Summary of the resulting equations for the three cases explored.

	Conditions	Resulting Equations
Case 1	Random waves along a flat bottom	$H_{RMS} = \frac{H_{0, RMS}}{1 + \beta x}; \beta = \frac{1}{3\sqrt{\pi}} C_D b_v N H_{0, RMS} k \frac{\sinh^3 kh + 3 \sinh kh}{(\sinh 2kh + 2kh) \sinh kh}$
Case 2	Random shallow water waves along a flat bottom	$H_{RMS} = H_{0, RMS} K_v; K_v = \frac{1}{1 + \frac{A_2}{m} H_{0, RMS}}; A_2 = \frac{C_D b_v N \alpha}{2\sqrt{\pi}}$
Case 3	Random shallow water waves along a sloping bottom	$H_{RMS} = H_{0, RMS} K_s K_v; K_s = \frac{h_o^{1/4}}{h^{1/4}}; K_v = \frac{1}{1 + 2 \frac{A_2}{m} H_{0, RMS} (K_s - 1)}; A_2 = \frac{C_D b_v N \alpha}{2\sqrt{\pi}}$

We then applied these models to the data, calculating C_D values for each case and vegetation zone. Not all waves were classified as shallow, particularly across the summer *S. foliosa* zone. We relaxed the criteria for shallow-water and included all waves in the analysis of the three cases. Simplifying the governing equations to assume shallow water waves resulted in a decrease in drag coefficients (Case 1 compared to Case 2). Allowing the water depth to vary with position, thus incorporating the effects of bottom slope, caused an increase in drag coefficients (Case 2 compared to Case 3). The values from Case 3 are, however, greater than those from Case 1, indicating the net effect of the inclusion of slope was an increase in wave height due to shoaling. By not including this wave-growth process, the attenuation is underestimated. Overall, the changes between the cases were small (less than 30%) for all zones. An example of the results from these cases for the summer transition zone is shown in Fig A1.

By including the effects of slope, the Case 3 C_D values are a more accurate representation of drag due to the presence of vegetation alone. These values can be considered conservative, since they also include the shallow water wave simplifications, which decrease the C_D values. Applying shallow simplifications also removes some dependence on wave parameters calculated from the wave statistics. Due to the increased accuracy and conservative nature of the method, the results from Case 3 are presented in the paper.

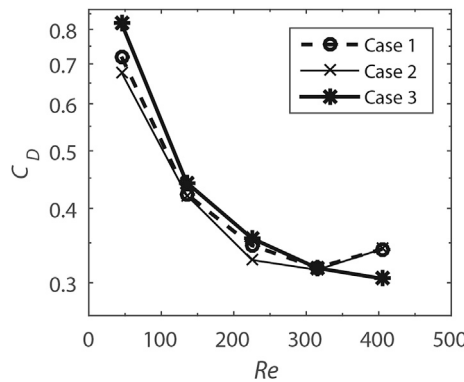


Fig. A1. C_D as a function of Re from the summer transition zone calculated with three different models; Case 1: Flat and not shallow; Case 2: Flat and shallow; Case 3: Sloped and shallow.

A2. Effect of bottom friction

We assessed the importance of bottom friction along the transect. We calculated C_D values adding bottom friction to the vegetation dissipation model as follows:

$$H_{RMS} = H_{0,RMS} K_s K_v K_f \tag{A12}$$

The K_f term is described in Section 2.4. We used a roughness length scale, k_b , of 0.01 m, which was measured in San Pablo Bay mudflats by Lacy and MacVean (2016). Including bottom friction caused a decrease in the C_D values by an average of 17%. The results for all vegetation zones were fit to the relationship $C_D = a + \left(\frac{b}{Re}\right)^c$ with and without the bottom friction term (Fig. A2). The 95% confidence intervals for these two fits overlap.

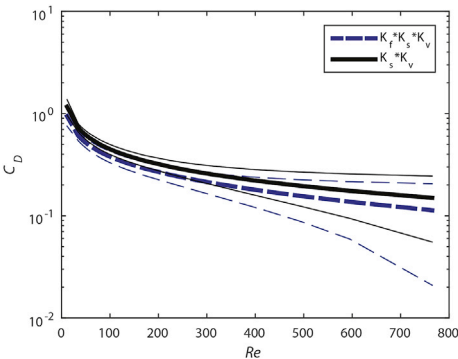


Fig. A2. C_D as a function of Re with (dashed blue line) and without (solid black line) including bottom friction. The thin lines show 95% confidence interval on the fits.

A3. $C_D - Re$ fit coefficients

Table A2 $C_D - Re$ fit coefficients				
$C_D = a + \left(\frac{b}{Re}\right)^c$	a	b	c	Range of Re
*Current study, <i>S. foliosa</i>	0.187	22.2	1.14	76–511
Current study, <i>S. pacifica</i>	0.402	11.9	1.53	10–170
Current study, Transition	−0.176	44.4	0.354	31–594
Möller et al., 2014 (irregular waves)	0.159	227.3	1.615	0–1200
**Jadhav et al., 2013	0.02	4000	0.78	200–3500
Pinsky et al., 2013	0	311.1	1.67	10–3000
Anderson and Smith, 2014	0.76	744.2	1.27	533–2296

*Fit to the summer dataset only. All others are a fit to both the winter and summer datasets.

**Obtained from Guannel et al. (2015).

Table A3 Correlation coefficients for the empirical fits to binned data.	
Vegetation type	r^2
<i>S. foliosa</i>	0.77
Transition	0.79
<i>S. pacifica</i>	0.93

References

Anderson, M.E., Smith, J.M., 2014. Wave attenuation by flexible, idealized salt marsh vegetation. *Coast. Eng.* 83, 82–92. <https://doi.org/10.1016/j.coastaleng.2013.10.004>.
Augustin, L.N., Irish, J.L., Lynett, P., 2009. Laboratory and numerical studies of wave damping by emergent and near-emergent wetland vegetation. *Coast. Eng.* 56, 332–340. <https://doi.org/10.1016/j.coastaleng.2008.09.004>.
Baye, P.R., 2012. Tidal marsh vegetation of China Camp, San Pablo Bay, California, San Franc. Estuary Watershed Sci. 10. <http://www.escholarship.org/uc/item/9r9527d7>.
Beagle, J., Salomon, M., Baumgarten, S., Grossinger, R., 2015. Shifting Shores: Marsh Expansion and Retreat in San Pablo Bay. San Francisco Estuary Institute, Richmond, CA.
Boesch, D.F., Turner, R.E., 1984. Dependence of fishery species on salt marshes: the role of food and refuge. *Estuaries* 7, 460. <https://doi.org/10.2307/1351627>.
Callaway, J.C., Josselyn, M.N., 1992. The introduction and spread of smooth cordgrass (*Spartina alterniflora*) in South San Francisco Bay. *Estuaries* 15, 218–226. <https://doi.org/10.2307/1352695>.
Callaway, J.C., Borgnis, E.L., Turner, R.E., Milan, C.S., 2012. Carbon sequestration and sediment accretion in San Francisco Bay tidal wetlands. *Estuar. Coast* 35, 1163–1181. <https://doi.org/10.1007/s12237-012-9508-9>.

Cloern, J.E., Nichols, F.H., 1985. Temporal Dynamics of an Estuary: San Francisco Bay. Springer Netherlands, Dordrecht. <http://public.eblib.com/choice/publicfullrecord.aspx?p=3103981>. (Accessed 26 June 2017).
Collins, J.I., 1972. Prediction of shallow-water spectra. *J. Geophys. Res.* 77, 2693–2707. <https://doi.org/10.1029/JC077i015p02693>.
Cooper, N.J., 2005. Wave dissipation across intertidal surfaces in the wash tidal inlet, Eastern England. *J. Coast Res.* 211, 28–40. <https://doi.org/10.2112/01002.1>.
Dalrymple, R.A., Kirby, J.T., Hwang, P.A., 1984. Wave diffraction due to areas of energy dissipation. *J. Waterw. Port. Coast. Ocean Eng.* 110, 67–79. [https://doi.org/10.1061/\(ASCE\)0733-950X\(1984\)110:1\(67\)](https://doi.org/10.1061/(ASCE)0733-950X(1984)110:1(67)).
Dean, R.G., Dalrymple, R.A., 1991. *Water Wave Mechanics for Engineers and Scientists*. world scientific publishing Co Inc.
Dhir, B., Sharmila, P., Saradhi, P.P., 2009. Potential of aquatic macrophytes for removing contaminants from the environment. *Crit. Rev. Environ. Sci. Technol.* 39, 754–781. <https://doi.org/10.1080/10643380801977776>.
Ellison, A.M., 1987. Effects of competition, disturbance, and herbivory on *Salicornia europaea*. *Ecology* 68, 576–586. <https://doi.org/10.2307/1938463>.
Fagherazzi, S., Gabet, E.J., Furbish, D.J., 2004. The effect of bidirectional flow on tidal channel planforms. *Earth Surf. Process. Landf* 29, 295–309. <https://doi.org/10.1002/esp.1016>.
Feagin, R.A., Irish, J.L., Möller, I., Williams, A.M., Colón-Rivera, R.J., Mousavi, M.E., 2011. Short communication: engineering properties of wetland plants with

- application to wave attenuation. *Coast. Eng.* 58, 251–255. <https://doi.org/10.1016/j.coastaleng.2010.10.003>.
- Ferner, M.C., 2012. Conclusion to the special issue: ecology and regional context of tidal wetlands in the San Francisco Bay national estuarine research Reserve, San Franc. *Estuary Watershed Sci.* 10, 1–5.
- Gedan, K.B., Kirwan, M.L., Wolanski, E., Barbier, E.B., Silliman, B.R., 2011. The present and future role of coastal wetland vegetation in protecting shorelines: answering recent challenges to the paradigm. *Clim. Change* 106, 7–29. <https://doi.org/10.1007/s10584-010-0003-7>.
- Goman, M., Malamud-Roam, F., Ingram, B.L., 2008. Holocene environmental history and evolution of a tidal salt marsh in San Francisco Bay, California. *J. Coast Res.* 24, 1126–1137.
- Green Infrastructure Effectiveness Database, 2017. National oceanic and atmospheric administration. <https://coast.noaa.gov/gisearch>.
- Guannel, G., Ruggiero, P., Faries, J., Arkema, K., Pinsky, M., Gelfenbaum, G., Guerry, A., Kim, C.-K., 2015. Integrated modeling framework to quantify the coastal protection services supplied by vegetation. *J. Geophys. Res. Oceans* 120, 324–345. <https://doi.org/10.1002/2014JC009821>.
- Herbers, T.H.C., Orzech, M., Elgar, S., Guza, R.T., 2003. Shoaling transformation of wave frequency-directional spectra. *J. Geophys. Res.* 108 <https://doi.org/10.1029/2001JC001304>.
- Infantes, E., Orfila, A., Simarro, G., Terrados, J., Luhar, M., Nepf, H., 2012. Effect of a seagrass (*Posidonia oceanica*) meadow on wave propagation. *Mar. Ecol. Prog. Ser.* 456, 63–72. <https://doi.org/10.3354/meps09754>.
- Jadhav, R.S., Chen, Q., Smith, J.M., 2013. Spectral distribution of wave energy dissipation by salt marsh vegetation. *Coast. Eng.* 77, 99–107. <https://doi.org/10.1016/j.coastaleng.2013.02.013>.
- Kirwan, M.L., Temmerman, S., Skeehan, E.E., Guntenspergen, G.R., Fagherazzi, S., 2016. Overestimation of marsh vulnerability to sea level rise. *Nat. Clim. Change* 6, 253–260. <https://doi.org/10.1038/nclimate2909>.
- Knutson, P.L., Brochu, R.A., Seelig, W.N., Inskeep, M., 1982. Wave damping in *Spartina alterniflora* marshes. *Wetlands* 2, 87–104. <https://doi.org/10.1007/BF03160548>.
- Kobayashi, N., Raichle, A.W., Asano, T., 1993. Wave attenuation by vegetation. *J. Waterw. Port, Coast. Ocean Eng.* 119, 30–48. [https://doi.org/10.1061/\(ASCE\)0733-950X\(1993\)119:1\(30\)](https://doi.org/10.1061/(ASCE)0733-950X(1993)119:1(30)).
- Lacy, J.R., MacVean, L.J., 2016. Wave attenuation in the shallows of San Francisco Bay. *Coast. Eng.* 114, 159–168. <https://doi.org/10.1016/j.coastaleng.2016.03.008>.
- Lacy, J.R., Allen, R.M., Foster-Martinez, M.R., Ferreira, J.C., O'Neill, A.C., 2017. Hydrodynamic and sediment transport data from San Pablo Bay and China Camp marsh (northern San Francisco Bay), 2013–2016, US Geol. Surv. Data Release. <https://doi.org/10.5066/F7HM56MX>.
- MacKenzie, R.A., Dionne, M., 2008. Habitat heterogeneity. *Mar. Ecol. Prog. Ser.* 368, 217–230.
- Mahall, B.E., Park, R.B., 1976. The ecotone between *Spartina foliosa* trin. and *Salicornia virginica* L. in salt marshes of Northern San Francisco Bay: I. Biomass and production. *J. Ecol.* 64, 421–433. <https://doi.org/10.2307/2258766>.
- Mendez, F.J., Losada, I.J., 2004. An empirical model to estimate the propagation of random breaking and nonbreaking waves over vegetation fields. *Coast. Eng.* 51, 103–118. <https://doi.org/10.1016/j.coastaleng.2003.11.003>.
- Méndez, F.J., Losada, I.J., Losada, M.A., 1999. Hydrodynamics induced by wind waves in a vegetation field. *J. Geophys. Res. Oceans* 104, 18383–18396. <https://doi.org/10.1029/1999JC900119>.
- Möller, I., Spencer, T., 2002. Wave dissipation over macro-tidal salt marshes: effects of marsh edge typology and vegetation change. *J. Coast Res.* 36, 506–521.
- Möller, I., Kudella, M., Rupprecht, F., Spencer, T., Paul, M., van Wesenbeeck, B.K., Wolters, G., Jensen, K., Bouma, T.J., Miranda-Lange, M., Schimmels, S., 2014. Wave attenuation over coastal salt marshes under storm surge conditions. *Nat. Geosci.* 7, 727–731. <https://doi.org/10.1038/ngeo2251>.
- Narayan, S., Beck, M.W., Reguero, B.G., Losada, I.J., van Wesenbeeck, B., Pontee, N., Sanchirico, J.N., Ingram, J.C., Lange, G.-M., Burks-Copes, K.A., 2016. The effectiveness, costs and coastal protection benefits of natural and nature-based defences. *PLoS One* 11, e0154735. <https://doi.org/10.1371/journal.pone.0154735>.
- Narayan, S., Beck, M.W., Wilson, P., Thomas, C., Guerrero, A., Shepard, C., Reguero, B.G., Franco, G., Ingram, C.J., Trespalacios, D., 2016. Coastal Wetlands and Flood Damage Reduction: Using Risk Industry-based Models to Assess Natural Defenses in the Northeastern USA. <https://doi.org/10.7291/v93x84kh>.
- Nielsen, P., 1992. Coastal Bottom Boundary Layers and Sediment Transport. World Scientific Publishing Co Inc.
- Nowacki, D.J., Beudin, A., Ganju, N.K., 2017. Spectral wave dissipation by submerged aquatic vegetation in a back-barrier estuary: wave dissipation by vegetation. *Limnol. Oceanogr.* 62, 736–753. <https://doi.org/10.1002/lno.10456>.
- Ouyang, X., Lee, S.Y., 2014. Updated estimates of carbon accumulation rates in coastal marsh sediments. *Biogeosciences* 11, 5057–5071. <https://doi.org/10.5194/bg-11-5057-2014>.
- Paquier, A.-E., Haddad, J., Lawler, S., Ferreira, C.M., 2016. Quantification of the attenuation of storm surge components by a coastal wetland of the US mid Atlantic. *Estuar. Coast.* <https://doi.org/10.1007/s12237-016-0190-1>.
- Pinsky, M.L., Guannel, G., Arkema, K.K., 2013. Quantifying wave attenuation to inform coastal habitat conservation. *Ecosphere* 4. <https://doi.org/10.1890/ES13-00080.1> art95.
- Pontee, N., Narayan, S., Beck, M.W., Hosking, A.H., 2016. Nature-based solutions: lessons from around the world. *Proc. Inst. Civ. Eng. Marit. Eng.* 169, 29–36. <https://doi.org/10.1680/jmaen.15.00027>.
- Rohrer, T., Kerr, D., Hogle, I., 2015. San Francisco estuary invasive *Spartina* project 2014 ISP monitoring and treatment report. Prep. Calif. State Coast. Conserv. San Franc. Invasive *Spartina* Proj. 1330.
- Schile, L.M., Callaway, J.C., Morris, J.T., Stralberg, D., Parker, V.T., Kelly, M., 2014. Modeling tidal marsh distribution with sea-level rise: evaluating the role of vegetation, sediment, and upland habitat in marsh resiliency. *PLoS One* 9, e88760. <https://doi.org/10.1371/journal.pone.0088760>.
- Spalding, M.D., McIvor, A.L., Beck, M.W., Koch, E.W., Möller, I., Reed, D.J., Rubinoff, P., Spencer, T., Tolhurst, T.J., Wamsley, T.V., van Wesenbeeck, B.K., Wolanski, E., Woodroffe, C.D., 2014. Coastal ecosystems: a critical element of risk reduction: coastal ecosystems and risk reduction. *Conserv. Lett.* 7, 293–301. <https://doi.org/10.1111/conl.12074>.
- Spalding, M.D., Ruffo, S., Lacambra, C., Meliane, I., Hale, L.Z., Shepard, C.C., Beck, M.W., 2014. The role of ecosystems in coastal protection: adapting to climate change and coastal hazards. *Ocean Coast Manag.* 90, 50–57. <https://doi.org/10.1016/j.ocecoaman.2013.09.007>.
- Sutton-Grier, A.E., Wowk, K., Bamford, H., 2015. Future of our coasts: the potential for natural and hybrid infrastructure to enhance the resilience of our coastal communities, economies and ecosystems. *Environ. Sci. Pol.* 51, 137–148. <https://doi.org/10.1016/j.envsci.2015.04.006>.
- Swanson, K.M., Drexler, J.Z., Schoellhamer, D.H., Thorne, K.M., Casazza, M.L., Overton, C.T., Callaway, J.C., Takekawa, J.Y., 2014. Wetland accretion rate model of Ecosystem resilience (WARMER) and its application to habitat sustainability for endangered species in the San Francisco estuary. *Estuar. Coast* 37, 476–492. <https://doi.org/10.1007/s12237-013-9694-0>.
- Swart, D.H., 1974. Offshore Sediment Transport and Equilibrium Beach Profiles. PhD Dissertation. Delft University of Technology.
- Takekawa, J., Thorne, K., Buffington, K., Spragens, K., Swanson, K., Drexler, J., Schoellhamer, D.H., Overton, C.T., Casazza, M.L., 2013. Final report for sea-level rise response modeling for San Francisco Bay estuary tidal marshes. <http://pubs.usgs.gov/of/2013/1081/pdf/ofr20131081.pdf>.
- Temmerman, S., De Vries, M.B., Bouma, T.J., 2012. Coastal marsh die-off and reduced attenuation of coastal floods: a model analysis. *Glob. Planet. Change* 92–93, 267–274. <https://doi.org/10.1016/j.gloplacha.2012.06.001>.
- Vuik, V., Jonkman, S.N., Borsje, B.W., Suzuki, T., 2016. Nature-based flood protection: the efficiency of vegetated foreshores for reducing wave loads on coastal dikes. *Coast. Eng.* 116, 42–56. <https://doi.org/10.1016/j.coastaleng.2016.06.001>.
- Wamsley, T.V., Cialone, M.A., Smith, J.M., Atkinson, J.H., Rosati, J.D., 2010. The potential of wetlands in reducing storm surge. *Ocean Eng.* 37, 59–68. <https://doi.org/10.1016/j.oceaneng.2009.07.018>.
- Wiberg, P.L., Sherwood, C.R., 2008. Calculating wave-generated bottom orbital velocities from surface-wave parameters. *Comput. Geosci.* 34, 1243–1262. <https://doi.org/10.1016/j.cageo.2008.02.010>.
- Windham, L., Weis, J., Weis, P., 2003. Uptake and distribution of metals in two dominant salt marsh macrophytes, *Spartina alterniflora* (cordgrass) and *Phragmites australis* (common reed). *Estuar. Coast Shelf Sci.* 56, 63–72. [https://doi.org/10.1016/S0272-7714\(02\)00121-X](https://doi.org/10.1016/S0272-7714(02)00121-X).
- Young, I.R., Babanin, A.V., 2006. The form of the asymptotic depth-limited wind wave frequency spectrum. *J. Geophys. Res.* 111 <https://doi.org/10.1029/2005JC003398>.
- Ysebaert, T., Yang, S.-L., Zhang, L., He, Q., Bouma, T.J., Herman, P.M.J., 2011. Wave attenuation by two contrasting Ecosystem engineering salt marsh macrophytes in the intertidal pioneer zone. *Wetlands* 31, 1043–1054. <https://doi.org/10.1007/s13157-011-0240-1>.